Chinese Chemical Letters 33 (2022) 3802–3808

Contents lists available at ScienceDirect

Chinese Chemical Letters

journal homepage: www.elsevier.com/locate/cclet

Remarkable-cycle-performance β-bismuthene/graphene heterostructure anode for Li-ion battery

Shouzheng Wang, Chunmei Tang*, Yu Huang, Jiangfeng Gong

College of Science, Hohai University, Nanjing 210098, China

ARTICLE INFO

Article history:
Received 14 September 2021
Revised 1 November 2021
Accepted 13 November 2021
Available online 18 November 2021

Keywords:
Anode material
Li-ion battery
Bismuthene
Graphene
Heterostructure
First-principles calculation

ABSTRACT

Remarkable Li-ion battery (LIB) anode materials need to have long cycle life and fast charge/discharge rate, however they are difficult to be realized in the monolayer anode materials. The monolayer β-Bi has the stiffness of only 33.0 N/m, thus the Bi/G heterostructure is proposed to improve the electronic and mechanical properties and to produce better LIB anode performance in this paper. The calculated results show that Bi/G heterostructure has excellent thermodynamic, dynamical and mechanical stability. The band gap is only 0.04 eV, which ensures remarkable electrical conductivity. In addition, the Bi/G heterostructure has higher stiffness (369.2 N/m) than that of monolayer β-Bi and graphene. The diffusion barrier ($E_{barrier}$) of 0.32 eV and volume expansion ratio (*VER*) of only 4% can ensure the rapid transport of Li^+ ions in the charge/discharge cycling process and long life of the LIB. These calculated theoretical results for describing the detail properties of Li storage and diffusion in the Bi/G heterostructure can supply adequate conclusive evidence for the prediction of remarkable properties of Bi/G heterostructure as an anode material for LIBs.

Human progress and social development cannot be separated from energy. The traditional energy(coal, oil, natural gas) is not only increasingly unable to meet the energy requirement of social development, but also lead to global greenhouse effect. In order to reduce greenhouse gas emissions from energy consumption and increase energy efficiency, several approaches are being proposed, including how to capture CO_2 more efficiently and convert it into other value-added products [1–3]. In addition, to explore new forms of renewable energy has become particularly urgent [4]. For example, wind energy, solar energy, electric energy, nuclear energy have been widely explored and developed in modern days. Li-ion battery (LIB) has been gradually become the major power source supplier basing on three point of advantages: firstly, high energy density; secondly, long cycle life and no memory effect; thirdly, friendly to the environment.

As an indispensable part of LIBs, excellent anode materials need to meet the following conditions: (1) The good thermodynamic and kinetic stability, which can ensure them to be able to withstand certain stress. (2) The suitable average adsorption energy (E_{ad}) of Li atoms should be ensured to be larger than 1.63 eV, which is defined as the cohesive energy of bulk Li on the experiment, while the E_{ad} should be also smaller than 3.0 eV [5–6]. (3) The formation of lithium dendrite will lead to battery failure and cause hidden danger of safety [7,8]. When the average open circuit voltage (OCV) should be fall in the energy range (0–2 V) during normal operation, then the Li dendrites formation will be well avoided [9,10]. (4) The smaller volume expansion ratio (VER) ($<$ 25%) can prevent the battery capacity from rapid degradation in the process of charging/discharging cycle, so that the battery has a longer cycle life [11,12].

In the develop history of LIB anode, graphite was used at the earliest time and has been successfully applied in commercial application recently. However, graphite anode has a low Li storage capacity (372 mAh/g) and poor cycling stability [13]. Although the Li storage capacity could be increased through alternative doping with light elements, it is rather difficult to be controlled by the experimental method. Later, pure metal alloy anodes appeared and usually had large Li storage capacities (Sb: 660 mAh/g [14], Si: 3580 mAh/g [15], Bi: 3800 mAh/g [16]), but the appeared large VER after plentiful Li atoms inserting and escaping (Sn: 260% [11], Si: 323% [15], Bi: 215% [11]) seriously reduce the cycle life of battery. Recently, two-dimensional (2D) nanomaterials have large surface area and good mechanical properties, so that they can withstand the stress in the process of deintercalation of Li without large deformation, which can increase the charge/discharge cycle life of battery, while the controllability of interlayer space can increase the capacity of Li storage [17]. As early in 2016, Zhang *et al.*

* Corresponding author.
E-mail address: tcmnj@163.com (C. Tang).

https://doi.org/10.1016/j.cclet.2021.11.037
1001-8417/

have proposed that β-Bi was the most stable phase of bismuthene [18]. Monolayer β-Bi has a narrower band gap (0.48 eV) than that of many other 2D monolayer nanomaterials, such as monolayer arsenene (1.94 eV) [19], monolayer ZrS_2 (1.63 eV) [20], β-antimonene (β-Sb) monolayer (1.24 eV) [21]. Most importantly, the monolayer 2D-Bi has been researched by Muhammad *et al.* that it had many advantages concluding small OCV, low diffusion energy barrier ($E_{barrier}$) for the Li^+ ion, large Li storage capacity, thus, it will be a well LIB candidate [22].

In the actual LIB application, the practical anode material must be bulk material or multilayer 2D material, the choice of above material maybe due to the reason that they can effectively slow down the VER to the largest level during the lithiation/delithiation cycle course and effectively improve the cycle life of LIBs to the longest [16]. Therefore, the study of multilayer structures as anode materials for LIBs attracts our attention. For example, it has been reported that in 2017 Su *et al.* have found that Bi@graphene nanocomposite was an effective anode material for Na-ion battery (NIB) [23]. As well known, among the multilayer structures, the van der Waals (vdW) heterostructure is one concerned kind of multilayer structure made up of different monolayers [24,25]. The heterostructure can combine the advantages of monolayer materials, while the disadvantages of materials can be eliminated. Recently, many different kinds of heterostructures have been proposed by researchers, such as phosphorene/grapheme [26], graphene/antimonene [27], graphene/WS_2 [28]. On the experiment, the β-bismuthene/grapheme (Bi/G) heterostructure has shown good performance as the anode material of NIB [29]. Therefore, we consider combining monolayer β-Bi with graphene, thus obtain a Bi/G heterostructure, which can be expected to be the anode material for LIBs.

Whether the Bi/G heterostructure is suitable for LIB anode material? Due to the excellent mechanical and electrical properties of graphene, many researchers have started to construct heterostructure containing graphene, which can enhance the cycle life and energy storage capacity [30]. As early in 2017, F. Reis *et al.* have proposed that monolayer bismuthene can be grown on a silicon substrate [31]. Hence, in this paper, we confirm Bi/G heterostructure has excellent thermodynamic, dynamical and mechanical stability. The band gap is only 0.04 eV, which ensures the higher electrical conductivity. In addition, the Bi/G heterostructure has higher stiffness (369.2 N/m) than monolayer β-Bi and graphene (343.3 N/m). The $E_{barrier}$ of 0.32 eV and VER of 4% can ensure the rapid transport of Li^+ ions in the charge/discharge cycle and long cycle life of LIB. We believe that this research will accelerate the experimental preparation and future development of LIB anode materials.

This paper use the Vienna *ab initio* simulation package (VASP) software [32,33]. Device Studio [34] program provides a number of functions for performing visualization, modeling and simulation. And simulation using VASP software integrated in Device Studio program. The Perdew-Burke-Ernzerhof (PBE) [35] functional basing on polarization generalized gradient approximation(GGA) is used [36,37]. The van der Waals interaction between layers still has an influence on the surface adsorption [35], so we adopt the DFT-D method proposed by Grimme to conduct dispersion correction [38]. The kinetic cutoff energy is set to be 500 eV. A perpendicular vacuum layer of 30 Å can eliminate the interlayer action. The k-point grid is in the Brillouin zone is $5 \times 5 \times 1$. The 10^{-6} eV and 0.01 eV/Å are separately the total energy convergence criterion and force convergence criterion.

The 2D monolayer β-Sb is calculated to verify the accuracy of above described method. The Sb-Sb bond length is calculated as 2.89 Å and similar to previous 2.87 Å [39]. The cohesive energy(the energy needed to isolate all the atoms inside a structure) of −4.24 eV/atom is similar to reported −4.26 eV/atom [39]. Obviously, the calculation method in this paper should be reliable.

For monolayer β-Bi and graphene, the optimized in-plane lattice constants are 4.20 Å and 2.47 Å respectively, which are very close to previous reported 4.26 Å [40] and 2.46 Å [41]. Monolayer β-Sb, β-Bi and graphene configurations are shown in Fig. S1 (Supporting information) and Table S1 (Supporting information). On the experiment, due to the existing influence of temperature and pressure, when two monolayer structures are stacked up, the mismatch problem must happen. Therefore, researchers must measure the mismatch ratio during the construction of heterostructures [42,43]. In fact, the smaller mismatch ratio, the more favorable growth of heterostructures. Usually the mismatch ratio should be ensured to be less than 5% [44,45]. After trying construct many different styles of grapheme and β-Bi, we find the smallest mismatch ratio of 1.8% appears for the heterostructure combined by the $\sqrt{3} \times \sqrt{3}$ supercell of graphene and 1×1 supercell of monolayer β-Bi (atomic number ratio is 3/1), 2×2 supercell are performed again on the constituted heterostructure, and the lattice constant after supercell is finally obtained $a = b = 8.53$ Å as shown in Fig. 1a. By calculating the energy for the Bi/G heterostructure with the interlayer space in the range from 3 Å to 4 Å, it is found in Fig. 1b that when the interlayer distance of above configurations is 3.36 Å, it has the lowest energy, which is as same as that of the optimized structure.

In the Bi/G heterostructure, compared with the original monolayer, the interlayer weak vdW interaction should not be negligible, thus, in practical application, the energy under the strain should be considered [46,47]. In the heterostructure, the strain on monolayer β-Bi and graphene is 3.2% and −0.6% respectively. The formation energy (E_{form}) is the energy released/absorbed by two monolayers to form a heterostructure. The stability of Bi/G heterostructure can be determined by calculating the E_{form} as follows [48]:

$$E_{form} = (E_{strained\ \beta-Bi} + E_{strained\ graphene} - E_{Bi/G})/A \quad (1)$$

where, $E_{strained\ \beta\text{-Bi}}$, $E_{strained\ graphene}$ and $E_{Bi/G}$ are the total energy of strained monolayer β-Bi, strained graphene, and Bi/G heterostructure, the supercell area is defined as A. The positive E_{form} indicates the exothermic and spontaneous formation process of heterostructure, which explores that the Bi/G heterostructure can be synthesized experimentally [49]. It is calculated that the E_{form} of Bi/G heterostructure is 22.1 meV/Å^2, which is larger than the interlayer binding energy and exfoliation energy of most materials (13–21 meV/Å^2) [50], such as G/WS_2 (20.0 meV/Å^2) [28], G/Sb (18.7 meV/Å^2) [27] and so on, indicating Bi/G heterostructure can be easily synthesized.

Average binding energy (E_b) per C atom can be used to analyze the stability of the graphene based heterostructure. Positive value indicates the stability of structure and explores its exothermal synthesis [51]. To further judge the stability of Bi/G heterostructure, we calculate E_b as follows [28]:

$$E_b = (E_{strained\ \beta-Bi} + E_{strained\ graphene} - E_{Bi/G})/N \quad (2)$$

where, N is the number of carbon atoms. Positive E_b indicates that the atomic binding process of heterostructure is exothermic and spontaneous. It is calculated that the E_b of Bi/G heterostructure is 57.9 meV, which is higher than that of many other heterostructures, such as G/MoS_2 (23 meV) [52], G/WS_2 (51.8 meV) [28]. Obviously, the larger value of $>E_b$, the more stable of the structure, hence the Bi/G heterostructure should be very stable.

As the anode material of LIBs, the dynamical stability is essential. We can prove that the Bi/G heterostructure should be dynamical stable by the fact that the phonon spectrum [53] shown in Fig. 2a has no virtual frequency. This figure combines the phonon spectrum characteristics of grapheme [54] and monolayer β-Bi. Therefore, the Bi/G heterostructure is kinetically stable.

The thermodynamic stability of Bi/G heterostructure can further be verified by the ab initio molecular dynamics (AIMD) simulation [33]. The temperature is set as 300 K. The total simulation time

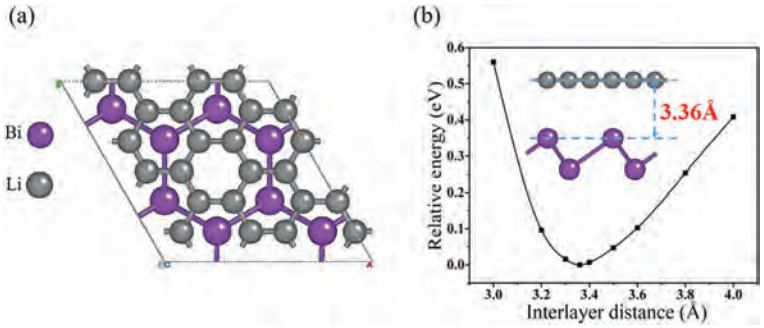

Fig. 1. (a) Top view and (b) side view and interlayer distances for Bi/G heterostructure.

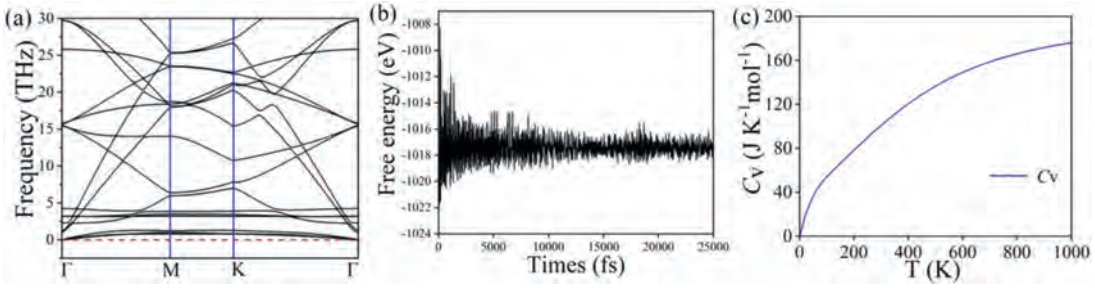

Fig. 2. (a) The phonon spectra, (b) variation of free energy over 25 ps during AIMD at 300 K and (c) the C_v of Bi/G heterostructure.

of free energy evolution is 25 ps, and 1 fs time step in the evolution process is carried. Obviously, as shown in Fig. 2b, the image shows that the structure of Bi/G heterostructure is still intact after 25 ps, and the energy tends to be flat, so it proves that the Bi/G heterostructure is thermodynamic stable. Therefore, we can also prove that a multilayer heterostructure composed of stable monolayer structures should be also stable, such as graphene/WS_2 [28], graphene/antimonene [27].

The C_v is the heat capacity per mole constant volume of atoms, which can further analyze the structural thermodynamic stability [55]. The C_v of Bi/G heterostructure is calculated as follows [56]:

$$C_V = \sum_{q\nu} k_B \left(\frac{\hbar w(q\nu)}{k_B}\right)^2 \frac{\exp(\hbar w(q\nu)/k_B T}{\left[\exp\left(\frac{\hbar w(q\nu)}{k_B T}\right) - 1\right]^2} \tag{3}$$

where, the Boltzmann constant (k_B) and Planck constant ($\hbar$) are used. w, q, v and T are frequency, wave vector, band index and temperature respectively. As shown in Fig. 2c, with the increase of temperature, the value of C_v gradually tends to be flat, which indicates that Bi/G heterostructure has certain thermodynamic stability and also be consistent with the AIMD calculation above, further demonstrates its feasibility as anode material for LIBs.

Generally, during the process of Li embedding/de-embedding in the battery, the surface of the material will be squeezed and deformed, which will reduce the cycling stability and service life of LIB. It is essential that the anode material should have excellent deformation resistance ability. Therefore, by calculating the elastic constant (C_{ij}) and Young's modulus (Y) of material, we can analyze the mechanical stability of the material and judge whether it is suitable for the LIB anode materials [57]. As well known, to measure the elastic constant C_{ij} on the experiment is usually difficult, thus the C_{ij} value only be calculated by the theoretical method. The thickness of the 2D material can be ignored, and the force will keep same along the thickness direction and is parallel to the surface. In the entire thin plane, three plane stress components σ_z, τ_{yz}, τ_{xz} at all points are all equal to zero, leaving σ_x, σ_y and τ_{xy} three plane stress components, hence the following 6 × 6 matrix for testing the elastic coefficient can be simplified as 3 × 3:

$$\begin{bmatrix}\sigma_x\\ \sigma_y\\ \sigma_z\\ \tau_{xy}\\ \tau_{yz}\\ \tau_{zx}\end{bmatrix} = \begin{bmatrix}C_{11} & C_{12} & C_{13} & C_{14} & C_{15} & C_{16}\\ C_{21} & C_{22} & C_{23} & C_{24} & C_{25} & C_{26}\\ C_{31} & C_{32} & C_{33} & C_{34} & C_{35} & C_{36}\\ C_{41} & C_{42} & C_{43} & C_{44} & C_{45} & C_{46}\\ C_{51} & C_{52} & C_{53} & C_{54} & C_{55} & C_{56}\\ C_{61} & C_{62} & C_{63} & C_{64} & C_{65} & C_{66}\end{bmatrix}\begin{bmatrix}\varepsilon_x\\ \varepsilon_y\\ \varepsilon_z\\ \gamma_{xy}\\ \gamma_{yz}\\ \gamma_{zx}\end{bmatrix} \tag{4}$$

$$\Rightarrow \begin{bmatrix}\sigma_x\\ \sigma_y\\ \tau_{xy}\end{bmatrix} = \begin{bmatrix}C_{11} & C_{12} & 0\\ C_{21} & C_{22} & 0\\ 0 & 0 & C_{44}\end{bmatrix} \times \begin{bmatrix}\varepsilon_x\\ \varepsilon_y\\ \gamma_{xy}\end{bmatrix}$$

Based on the symmetry of the geometric structure, the formula of elastic coefficient matrix can be simplified as follows [49]:

$$C_{ij} = \left[\frac{\partial\sigma(\varepsilon_j)}{\partial\varepsilon_i}\right]_{\varepsilon=0} = \begin{bmatrix}C_{11} & C_{12} & 0\\ C_{12} & C_{22} & 0\\ 0 & 0 & C_{44}\end{bmatrix} \tag{5}$$

where, C_{11} and C_{22} in the matrix respectively represent the corresponding stiffness of 2D structure when the uniaxial tensile strain is along the x and y directions [58]. C_{12} and C_{44} respectively represent the ability of structure to resist external biaxial strain and the resistance to deformation under in-plane shear strain. In the symmetric elastic coefficient matrix, $C_{12} = C_{21}$, $C_{11} = C_{22}$ [49].

The Y can be calculated as follows [55]:

$$Y = \frac{(C_{11}^2 - C_{12}^2)}{C_{11}} \tag{6}$$

The C_{11} and C_{12} should meet criteria (1) $C_{11} > |C_{12}|$ and (2) $C_{11} > 0$ [59,60]. It can be seen from Table 1 that the monolayer β-Bi, graphene and Bi/G heterostructure are all mechanically stable. According to the calculated results in Table 1, they are all mechanically stable, and the elastic constant of Bi/G heterostructure (369.2 N/m) is much greater than that of monolayer β-Bi (33.0 N/m) and graphene (343.3 N/m). This shows that the weak interaction between monolayer β-Bi and graphene increases the elastic constant of Bi/G heterostructure. To verify the correctness of calculated results, we compare the calculated Y of monolayer β-Bi and graphene with previous results, and find they are very close

Table 1.
The C_{ij} and Y of monolayer β-Bi, graphene, and Bi/G heterostructure.

System	C_{11}	C_{22}	C_{12}	Y (N/m)
β-Bi	34.7	34.7	7.7	33.0 26.3 [61]
Graphene	354.1 352.7	354.1 352.7	61.7 60.9	343.3 342.2 [62] 340 ± 50 [63]
Bi/G	384.3	384.3	76.1	369.2

to previous reported values (26.3 N/m and 342.2 N/m) [61,62], and are also within the error range of experimental value (340 ± 50 N/m) [63]. The Y of Bi/G heterostructure is larger than that of many structures, such as Ge (41.4 N/m) [64], Si (60.6 N/m) [62], BP (23.2 N/m) [49], and Ti_2C (130 N/m) [65]. Therefore, the Bi/G heterostructure has high mechanical stability and can resist to the deformation brought by the inserting and escaping of external numerous Li atoms.

Electronic conductivity is one of the important criteria to judge whether a material is suitable for the anode materials of LIBs. In many reported references, the electrical conductivity of the considered material is judged mainly by the band gap of energy bands. For example, G/MoS_2 has a narrower band gap and higher conductivity than that of MoS_2 [30]. Cu_2O gradually increases electronic conductivity as the band gap narrows [66]. The semiconductor PbS with the narrow band gap is combined with CeO_2, which can further decrease the band gap and enhance electrical conductivity [67]. Band gaps of La and Pb doped $SrSnO_3$ are narrowed and their electrical conductivity are enhanced [68]. In order to study the electronic properties of heterostructures, we calculate the energy bands of monolayer β-Bi, graphene and Bi/G heterostructure and show them in Fig. S2 (Supporting information). The monolayer β-Bi has a direct band gap of 0.48 eV, so it should be a semiconductor. The graphene has a zero band gap, indicating its metallic property, which is consistent with previous studies [69]. The band gap of Bi/G heterostructure is only 0.04 eV, indicating that the introduction of graphene can reduce the band gap of heterostructure and effectively improve the electrical conductivity.

Based on above analysis of dynamic stability, thermodynamic stability, mechanical stability and ideal electrical conductivity of Bi/G heterostructure, we can preliminarily prove that Bi/G heterostructure has the potential to be used as anode material for LIB.

Li atoms are usually adsorbed on the surface of 2D materials, and the strength of adsorption can be reflected by adsorption energy (E_{ad}). The larger E_{ad} is, the stronger adsorption strengthen of Li atoms on the surface will be. The ideal E_{ad} should be between 1.63 eV∼3.0 eV [5,6]. The E_{ad} of Li atom is a very important index for the anode materials of LIBs. In fact, Li atom can be located above grapheme (Li/G/Bi), between graphene and β-Bi layer (G/Li/Bi), and below β-Bi layer (G/Bi/Li). It is well known that the site above the six-member ring center of graphene should be the most stable for adsorbed atom [70], and many different possible adsorption sites for external atom on monolayer β-Bi have also been discussed [22]. Therefore, as shown in Fig. S3 (Supporting information), there are seven adsorption sites for the Li atom in Bi/G heterostructure, that is, site A_1 is above the center of 6-Bi ring and 6-C ring, site B_1 is above the center of 6-C ring and above concave Bi atom, site C_1 is above the center of 6-C ring and the bulge Bi atom, site A_2 is below the center of 6-C ring and above the center of the 6-Bi ring, site B_2 is below the center of the 6-C ring and above the concave Bi atom, site A_3 is below the center of 6-Bi ring and 6-C ring, site B_3 is below the center of 6-C ring and below bulge Bi atom.

The following formula is carried to calculate the E_{ad} for the Li in Bi/G heterostructure [71]:

$$E_{\mathrm{ad}} = E_{Li} + E_{substrate} - E_{total} \tag{7}$$

where, the energy of isolated Li is defined as E_{Li}, which is applied for calculating the E_{ad} of Li^+ ion in many reported calculations [21-22,72]. The greater positive E_{ad} indicates that Li atom can be adsorbed on Bi/G heterostructure more stably. The E_{ad} of one Li in the Bi/G heterostructure are 1.72 eV (site A_1), 1.72 eV (site B_1), 1.71 eV (site C_1), 2.62 eV (site A_2), 2.80 eV (site B_2), 2.24 eV (site A_3), and 2.17 eV (site B_3), separately. Therefore, the most stable position for Li atom should be between two monolayers, which is caused by the interaction between layers of the heterostructure [73], and as same as that of the Li atom on G/WS_2 [28] and G/Sb [27]. The E_{ad} of one Li atom at site B_2 is larger than that on monolayer β-Bi (2.70 eV) [22] and graphene (1.69 eV) [74], which indicates that the Bi/G heterostructure for adsorption of Li atom at site B_2 has remarkable stability. The E_{ad}s at seven sites are all in the range of 1.63–3.0 eV [5,6], indicating the possibility of the Bi/G heterostructure applied for suitable LIB anode material. Due to the synergistic effect, Bi/G heterostructure can effectively enhance the adsorption strength of Li atoms. In addition, Li atoms are more likely to be inserted between layers of Bi/G heterostructure, rather than on top of graphene or under monolayer β-Bi, and the ability to insert atoms directly into layers of heterostructure has been demonstrated experimentally [75,76].

One performance indicator of LIBs is the charge/discharge rate, and the E_{barrier} of the Li^+ ion will have a direct impact on it. The E_{barrier} for Li^+ ion along all possible diffusion paths in Bi/G heterostructure have been calculated. The nudged-elastic-band (NEB) method is used to verify the E_{barrier} of one Li^+ ion between two adjacent adsorption sites in the Bi/G heterostructure, and the minimum-energy-paths (MEP) is used to verify the E_{barrier} [77]. As we know, the energy required for the vertical diffusion of ions through the layers is much higher than that for the parallel diffusion between layers, so we only discuss the parallel diffusion path between layers for the Li^+ ion here [31]. Combined with the structural characteristic of Bi/G heterostructure, we calculate the E_{barrier}s of Li^+ ions along ten parallel diffusion paths, that is, Path 1: $B_1 \rightarrow A_1 \rightarrow C_1$, Path 2: $B_2 \rightarrow A_2 \rightarrow B_2$, Path 3: $B_3 \rightarrow A_3 \rightarrow B_3$, Path 4: $A_1 \rightarrow A_1$, Path 5: $B_1 \rightarrow B_1$, Path 6: $C_1 \rightarrow C_1$, Path 7: $A_2 \rightarrow A_2$, Path 8: $B_2 \rightarrow B_2$, Path 9: $A_3 \rightarrow A_3$, Path 10: $B_3 \rightarrow B_3$. Among them, paths 1, 4, 5, 6 are above the graphene layer, paths 2, 7, 8 are in the middle of Bi/G heterostrature, and paths 3, 9, 10 are below the β-Bi layer. Finally three kinds of lowest parallel diffusion paths (Path 1: $B_1 \rightarrow A_1 \rightarrow C_1$, Path 2: $B_2 \rightarrow A_2 \rightarrow B_2$, Path 3: $B_3 \rightarrow A_3 \rightarrow B_3$) between each layer are selected.

The E_{barrier} of one Li^+ ion diffusion in a certain path in Bi/G heterostructure can be gotten follow the formula [78]:

$$E_{barrier} = E_{TS} - E_{SS} \tag{8}$$

here, the energy of the transitional state (E_{TS}) and most stable state (E_{ss}) for one Li atom adsorbed Bi/G heterostructure are introduced. All diffusion paths and the E_{barrier}s for the Li^+ ion are shown in Figs. 3a-c. It is clear that the E_{barrier} of the Li^+ ion diffusion along path 3 is the lowest (0.32 eV), while that of the Li^+ ion diffusion along path 1 and path 2 are 0.38/0.37 eV and 0.41 eV, respectively. Obviously, the minimum E_{barrier} of the Li^+ ion in the Bi/G heterostructure is smaller than that of many other monolayer anode materials, such as $Ti_3C_2(OH)_2$ (1.02 eV) [79], InP_3 (0.73 eV) [80], SnS_2 (0.69 eV) [81] and so on. Therefore, Bi/G heterostructure can ensure the fast charge/discharge rate for the anode material of LIB.

The excellent diffusion property of Li^+ ion in the Bi/G heterostructure can be further verified by calculating the diffusion coefficient (D), which can be obtained by calculating the following

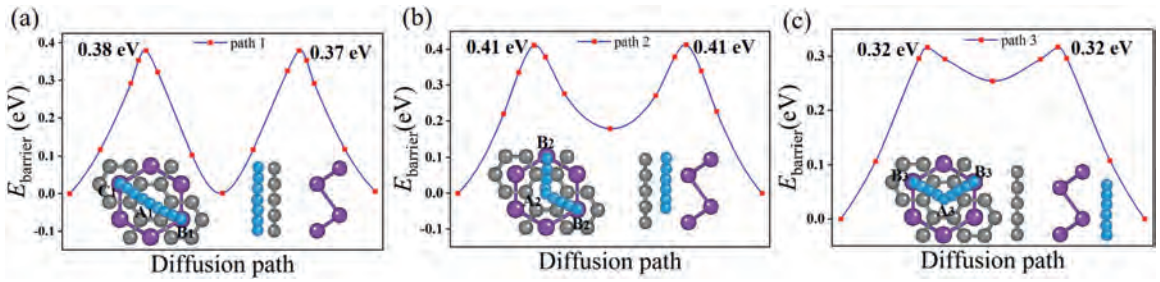

Fig. 3. Top view and side view of three diffusion paths; $E_{barrier}$ of one Li atom along (a) path 1 on graphene, (b) path 2 in the interlayer of Bi/G heterostructure and (c) path 3 below the β-Bi layer.

formula [82]:

$$D \approx \exp(\frac{E_{barrier}}{kT}) \quad (9)$$

where, k is the Boltzman constant and T presents the temperature. It can be calculated that the diffusion coefficient of Li^+ ion in the Bi/G heterostructure is about $10^6/10^7$ times faster than that for the Li^+ ion in the SnS_2/InP_3 heterostructure at 300 K [80,81].

The interaction mechanism between Li and Bi/G heterostructure is studied by analyzing the PDOS of one Li atom adsorbed Bi/G heterostructure, which is shown in Fig. S4 (Supporting information). By the Lorentzian extension of discrete energy levels, the weight of PDOS is given by the sum of orbital population for the energy levels. In the figure, the black dotted line at 0 eV is Fermi energy (E_f). The PDOS of Bi/G heterostructure mainly distributes between −14 eV and 4 eV, and that of Bi(s), Bi(p) and C(p) orbitals show continuous distribution. It is mainly reflected that the PDOS of Bi(s) is mainly from −13 eV to −8 eV, that of Bi(p) distribute from −4 eV to 4 eV, and that of C(p) starts from −14 eV to 5 eV Compared with the system without adsorbing a Li atom, the PDOS shift significantly from right to left after adsorption of Li, indicating the metallic system is formed. In the range from −4 eV to 3 eV, the orbital of Li(s) overlaps with that of Bi(p) obviously, which indicates that there is a certain hybridization between them. According to the peak height of the PDOS for Li(s) orbital in the hybridization energy range occupied by electrons below E_f, the hybridization effect of Li atom in G/Li/Bi structure and G/Bi/Li structure are significantly greater than that of Li/G/Bi structure. Combined with the PDOS area distribution of Li(s) orbital, it can be known that the hybridization effect of G/Li/Bi structure is the most obvious. Therefore, the hybridization strengthen between Li atom and Bi/G heterostructure is arranged in the order of G/Li/Bi > G/Bi/Li > Li/G/Bi, which is consistent with the E_{ad} of Li atom at different positions in Bi/G heterostructure.

The adsorption of multilayer Li atoms in Bi/G heterostructure is calculated, we use the following formula to calculate the average adsorption energy for each layer Li atoms (E_{ad}(n)) [71]:

$$E_{ad}(n) = (E_{Bi/G+(n-1)Li} + \mu E_{Li} - E_{Bi/G+nLi})/\mu \quad (10)$$

where, n represent the adsorbed total Li atom number, μ indicates the Li atom in the corresponding n^{th} layer, respectively. According to calculated E_{ad} for the isolated Li atom, in the Bi/G heterostructure, the first Li layer atoms should be adsorbed at the most stable B_2 site. When locating the second layer Li atoms, they should be located at site A_2 according to the second largest E_{ad}. However, because the Bi/G heterostructure has the interlayer spacing of only 3.36 Å, which is not big enough to accommodate the second layer of Li atoms in the vertical interlayer space. In order to accommodate more layers of Li atoms as stably as possible, after the trying of locating second layer Li atoms at any sites above the upper layer and below the low layer, site B_3 below the β-Bi layer are ultimately most stable for the adsorbed Li atoms in the optimized structure, where can support comfortable space for Li atoms. The optimized structure of four Li layers adsorbed Bi/G heterostructure is shown in Fig. 4a. As for the third layer Li atoms, by optimizing the structure with Li atoms at different positions above the upper layer and below the lower layer, many structures are seriously destroyed, only the site C_1 above the graphene are stable for the third Li layer adsorption. Then, for the fourth layer of Li atoms, the stable adsorption site X (below the most stable adsorption site B_2) is finally selected known from many optimized structures with Li atoms at different sites above the upper layer and below the lower layer. The E_{ad}(n) of first to fourth Li layer in the Bi/G heterostructure are calculated as 2.64, 2.23, 1.70, 1.86 eV respectively, which fall in the experimental cohesive energy range of bulk Li (1.63–3.0 eV).

The OCV is an important property of anode materials for LIBs. Usually, a smallest OCV for anodes in LIBs can get a maximum voltage [71,83]. The OCV of Bi/G heterostructure is calculated as follows [10]:

$$OCV = (E_{Bi/G} + nE_{bcc-Li} - E_{Bi/G+nLi})/ne \quad (11)$$

where, n and e are the adsorbed Li atom number and charge of an electron respectively. Obviously, as the number of adsorbed Li atoms gradually increases, the value of OCV is gradually decreasing, as shown in Fig. 4b. When the value of OCV decreases to 0 V, Bi/G heterostructure reaches the maximum theoretical Li storage capacity. When adsorbing fourth layers of Li atoms, the OCV value is 0.08 V. Thus, introducing more Li atoms will turn the OCV value to negative, and the lowest OCV value is 0.08 V. The corresponding average OCV value is 0.32 V, which meets the requirement (0–0.8 V) and can effectively prevent the formation of dendrite [84]. Obviously, the OCV of Bi/G heterostructure is lower than that of many other structures, such as graphdiyne (0.64 V) [85], monolayer MoC (0.63 V) [86] and monolayer InP_3 (0.53 V) [80], which indicates that Bi/G heterostructure can make the battery have higher efficiency and become a suitable choice for LIB anode.

More 2D materials are used as anode materials for LIBs. One reason is that the VER of pure alloy materials will be too high, which will reduce the service life of LIBs. The VER can effectively measure the service life of LIBs. The smaller VER means the smaller deformation of structure in the charge/discharge process, thus improving the cycle life of LIBs. The maximum VER of Bi/G heterostructure is only 4%, which is far lower than the 25% setted by the experiment researchers [87] and that of the Bi alloy (215%) [11], indicating that Bi/G heterostructure should be a very suitable anode material for LIBs.

The maximum theoretical Li storage capacity of Bi/G heterostructure is calculated as follows [88]:

$$C = n\nu F 10^3/M_C \quad (12)$$

M_c is the molar weight of Bi/G heterostructure, and ν is the Li valency. The Faraday constant F is 26.801 Ah/mol [88]. Compared with some lightweight materials, Bi/G heterostructure has a very

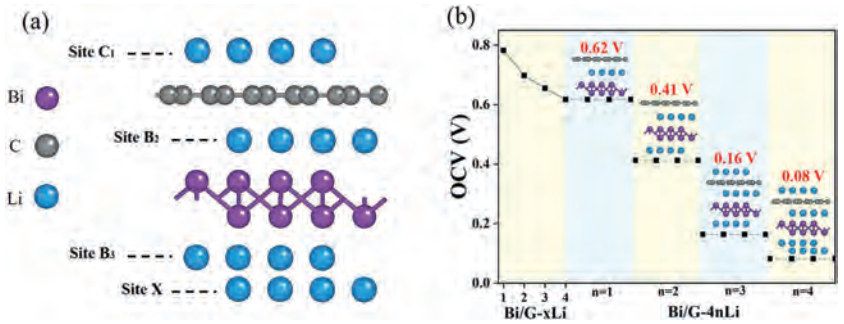

Fig. 4. (a) Side view of Bi/G heterostructure with four-layer Li atoms. (b) The OCV of Bi/G-xLi (x = 1–4) and Bi/G-4n Li (n = 1–4).

heavy relative atomic mass, so the largest theoretical Li storage capacity of BiC_3Li_2 is 218.69 mAh/g, but significantly reduces the VER and increases the cycle life. Therefore, many monolayer metal materials have been used as anode materials for LIBs, such as GeS (256 mAh/g) [89], InP_3 (258.1 mAh/g) [80] and SnS_2 (293 mAh/g) [81].

The adsorption characteristics can be further studied by calculating the electron localization function (ELF) on plane (110). Fig. S5 (Supporting information) shows the Bi/G heterostructure with the adsorption of one to four layers Li atoms. It can be seen from the figure that when the first Li layer is adsorbed, the electrons around Li atoms have a large negative electron cloud, which can provide a good environment for the adsorption of Li atoms. After four layers of Li atoms are adsorbed, it can be seen that the electron density in the outermost layer is very high, showing orange or even red, which means that it can no longer continue to adsorb Li atoms. This is consistent with previous calculated E_{ad}(n) and OCV.

In conclusion, the 0.04 eV band gap of the Bi/G heterostructure is much narrower than that of monolayer β-Bi (0.48 eV), indicating that the Bi/G heterostructure has higher electrical conductivity, which can provide faster electron transport rate for the lithiation/delithiation process of the battery. Compared with the monolayer β-Bi, the Bi/G heterostructure has higher E_{ad} for Li atom. The low $E_{barrier}$ (0.32 eV) makes it possible for Li^+ ion to diffuse rapidly during charge/discharge course. The stiffness of Bi/G heterostructure is 369.2 N/m, while the maximum *VER* after maximum Li atoms adsorption is only 4%, which makes the LIB more stabler and longer cycle life. Considering that the Bi/G heterostructure has higher electronic conductivity, stronger adsorption capacity of Li atom, lower $E_{barrier}$ for the Li^+ ion, better stability and smaller VER, which shows that it is a very suitable anode material for LIBs.

Declaration of competing interest

The authors declare that they have no known competing financial interests or personal relationships that could have appeared to influence the work reported in this paper.

Acknowledgments

This work was partially supported by the postgraduate research opportunities program of HZWTECH (No. HZWTECH-PROP) and financially sponsored by the Fundamental Research Funds for the Central Universities (No. B210203059), National Natural Science Foundation of China (No. 22075068).

Supplementary materials

Supplementary material associated with this article can be found, in the online version, at doi:10.1016/j.cclet.2021.11.037.

References

[1] M. Armand, J.M. Tarascon, Nature 451 (2008) 652–657.
[2] H.Y. Yang, C.Z. Hea, L. Fu, et al., Chin. Chem. Lett. 32 (2021) 3202–3206.
[3] L. Fu, R. Wang, C.X. Zhao, et al., Chem. Eng. J. 414 (2021) 128857.
[4] R. Wang, C.Z. He, W.X. Chen, C.X. Zhao, J.R. Huo, Chin. Chem. Lett. 32 (2021) 3821-3824.
[5] M. Hankel, D.J. Searles, Phys. Chem. Chem. Phys. 18 (2016) 14205–14215.
[6] H.J. Hwang, J. Koo, M. Park, et al., J. Phys. Chem. C 117 (2013) 6919–6923.
[7] Z.Y. Zeng, W.I. Liang, H.G. Liao, et al., Nano Lett. 14 (2014) 1745–1750.
[8] Z.Y. Zeng, P. Barai, S.Y. Lee, et al., Nano Energy 72 (2020) 104721.
[9] A. Eftekhari, Energy Storage Mater. 7 (2017) 157–180.
[10] B. Jang, J. Koo, M. Park, et al., Appl. Phys. Lett. 103 (2013) 263904.
[11] W.J. Zhang, J. Power Sources 196 (2011) 13–24.
[12] H. Wu, Y. Cui, Nano Today 7 (2012) 414–429.
[13] J.R. Dahn, T. Zheng, Y.H. Liu, J.S. Xue, Science 270 (1995) 590–593.
[14] M. He, K. Kravchyk, M. Walter, M.V. Kovalenko, Nano Lett. 14 (2014) 1255–1262.
[15] J.C. Arrebola, A. Caballero, J.L. Gómez-Cámer, et al., Electrochem. Commun. 11 (2009) 1061–1064.
[16] Y.X. Huang, C.Y. Zhu, S.L. Zhang, et al., Nano Lett. 19 (2019) 1118–1123.
[17] L.W. Ji, Z. Lin, M. Alcoutlabi, X.W. Zhang, Energy Environ. Sci. 4 (2011) 2682–2699.
[18] S.L. Zhang, M.Q. Xie, F.Y. Li, et al., Angew. Chem. Int. Edit. 55 (2016) 1666–1669.
[19] D. Kecik, E. Durgun, S. Ciraci, Phys. Rev. B 94 (2016) 205409.
[20] Y. Li, J. Kang, J.B. Li, RSC Adv. 4 (2014) 7396–7401.
[21] X.X. Wang, C.M. Tang, X.F. Zhou, W.H. Zhu, L. Fu, Appl. Surf. Sci. 495 (2019) 143549.
[22] M.I. Khan, G. Nadeem, A. Majid, M. Shakil, Mater. Sci. Eng. B 266 (2021) 115061.
[23] D.W. Su, S.X. Dou, G.X. Wang, Nano Energy 12 (2014) 88–95.
[24] M.U. Rehman, C.Q. Hua, Y.H. Lu, Chin. Phys. B 29 (2020) 057304.
[25] X.W. Wang, C.C. Xiao, C. Yang, et al., Sci. Bull. 65 (2020) 1252–1259.
[26] G.C. Guo, D. Wang, X.L. Wei, et al., J. Phys. Chem. Lett. 6 (2015) 5002–5008.
[27] X.X. Wang, C.M. Tang, X.F. Zhou, W.H. Zhu, C. Cheng, Appl. Surf. Sci. 491 (2019) 451–459.
[28] M.Z. Zhang, C.M. Tang, W. Cheng, L. Fu, J. Alloy. Compd. 855 (2021) 157432.
[29] J. Zhou, J.C. Chen, M.X. Chen, et al., Adv. Mater. 31 (2019) 1807874.
[30] H.B. Shu, F. Li, C.L. Hu, et al., Nanoscale 8 (2016) 2918–2926.
[31] F. Reis, G. Li, L. Dudy, et al., Science 357 (2017) 287–290.
[32] P.E. Blöchl, Phys. Rev. B 50 (1994) 17953–17979.
[33] G. Kresse, J. Furthmüller, Phys. Rev. B 54 (1996) 11169–11186.
[34] Hongzhiwei Technology, Device Studio, Version 2021A, China (2021). Available online: https://iresearch.net.cn/cloudSoftware (accessed on 2021.09).
[35] J.P. Perdew, K. Burke, M. Ernzerhof, Phys. Rev. Lett. 77 (1996) 3865–3868.
[36] Y. Wang, J.P. Perdew, Phys. Rev. B 43 (1991) 8911.
[37] T. Georgiou, R. Jalil, B.D. Belle, et al., Nat. Nanotechnol. 8 (2012) 100–103.
[38] S. Grimme, J. Antony, S. Ehrlich, H. Krieg, J. Chem. Phys. 132 (2010) 154104.
[39] G.X. Wang, R. Pandey, S.P. Karna, ACS Appl. Mater. Inter. 7 (2015) 11490–11496.
[40] S.M. Mozvashi, S.I. Vishkayi, M.B. Tagani, Physica E 118 (2020) 113914.
[41] X.F. Fan, W.T. Zheng, J.L. Kuo, D.J. Singh, ACS Appl. Mater. Inter. 5 (2013) 7793–7797.
[42] J. Kang, J.B. Li, S.S. Li, J.B. Xia, L.W. Wang, Nano Lett. 13 (2013) 5485–5490.
[43] Y. Gao, Q.C. Liu, B.X. Xu, ACS Nano 10 (2016) 5431–5439.
[44] Y. Chen, J. Washburn, Phys. Rev. Lett. 77 (1996) 4046–4049.
[45] H. Ding, S.S. Dwaraknath, L. Garten, et al., ACS Appl. Mater. Inter. 8 (2016) 13086–13093.
[46] H.T. Liu, Z.Y. Huang, G. Wu, et al., J. Mater. Chem. A 6 (2018) 17040–17048.
[47] Y.R. Wang, Z.Y. Jiao, S.H. Ma, Y.L. Guo, J. Power Sources 413 (2019) 117–124.
[48] A.K. Geim, I.V. Grigorieva, Nature 499 (2013) 419–425.
[49] Q. Peng, K.M. Hu, B.S. Sa, et al., Nano Res. 10 (2017) 3136–3150.
[50] T. Björkman, A. Gulans, A.V. Krasheninnikov, R.M. Nieminen, Phys. Rev. Lett. 108 (2012) 235502.
[51] S. Naji, H. Zaari, A. Al–Ammari, A. Benyoussef, A. Ennaoui, Opt. Quant. Electron. 53 (2021) 49.
[52] Y.D. Ma, Y. Dai, M. Guo, C.W. Niu, B.B. Huang, Nanoscale 3 (2011) 3883–3887.

[53] X. Gonze, C. Lee, Phys. Rev. B 55 (1997) 10355–10368.
[54] G.J. Slotman, G.A.D. Wijs, A. Fasolino, M.I. Katsnelson, Ann. Phys-Berlin 526 (2014) 381–386.
[55] T.S. Zhao, S.H. Zhang, Y.G. Guo, Q. Wang, Nanoscale 8 (2016) 233–242.
[56] C.M. Tang, X.X. Wang, H.B. Yao, L. Fu, Mater, Today Commun. 25 (2020) 101587.
[57] E.S. Fisher, E. Dever, Acta. Metall. 18 (1970) 265–269.
[58] Q. Wei, X.H. Peng, Appl. Phys. Lett. 104 (2014) 251915.
[59] M. Maździarz, 2D Mater. 6 (2019) 048001.
[60] M. Born, K. Huang, M. Lax, Am. J. Phys. 23 (1955) 474.
[61] M. Jafari, R. Ansari, S. Rouhi, Superlattice. Microst. 140 (2020) 106476.
[62] R.C. Andrew, R.E. Mapasha, A.M. Ukpong, N. Chetty, Phys. Rev. B 85 (2012) 125428.
[63] C.G. Lee, X.D. Wei, J.W. Kysar, J. Hone, Science 321 (2008) 385–388.
[64] H.L. Zhang, R. Wang, Physica B 406 (2011) 4080–4084.
[65] S. Wang, J.X. Li, Y.L. Du, C. Cui, Comp. Mater. Sci. 83 (2014) 290–293.
[66] L.M. Zhang, L. McMillon, J. McNatt, Sol. Energ. Mat. Sol. C. 108 (2013) 230–234.
[67] B. Mohanty, A. Chattopadhyay, J. Nayak, J. Alloy. Compd. 850 (2021) 156735.
[68] Q. Gao, K.F. Li, L. Zhao, et al., ACS Appl. Mater. Inter. 11 (2019) 25605–25612.
[69] C.H. Xu, B.H. Xu, Y. Gu, et al., Energy Environ. Sci. 6 (2013) 1388–1414.
[70] Y.Y. Liu, V.I. Artyukhov, M.J. Liu, A.R. Harutyunyan, B.I. Yakobson, J. Phys. Chem. Lett. 4 (2013) 1737–1742.
[71] Q.Y. Zhang, C.M. Tang, W.H. Zhu, C. Cheng, J. Phys. Chem. C 122 (2018) 22838–22848.
[72] X.D. Lv, F.Y. Li, J. Gong, et al., Phys. Chem. Chem. Phys. 22 (2020) 8902–8912.
[73] A.A. Kistanov, D.R. Kripalani, Y. Cai, et al., J. Mater. Chem. A 7 (2019) 2901–2907.
[74] F. Yao, F. Güneş, H.Q. Ta, et al., J. Am. Chem. Soc. 134 (2012) 8646–8654.
[75] X. Huang, Z.Y. Zeng, H. Zhang, Chem. Soc. Rev. 42 (2013) 1934–1946.
[76] H.T. Yuan, H.T. Wang, Y. Cui, Acc. Chem. Res. 48 (2015) 81–90.
[77] G. Henkelman, H. Jonsson, J. Chem. Phys. 113 (2000) 9978–9985.
[78] S.T. Oyama, D. Lee, P. Hacarlioglu, R.F. Saraf, J. Membrane Sci. 244 (2004) 45–53.
[79] Q. Tang, Z. Zhou, P.W. Shen, J. Am. Chem. Soc. 134 (2012) 16909–16916.
[80] J. Liu, C.S. Liu, X.J. Ye, X.H. Yan, J. Mater. Chem. A 6 (2018) 3634–3641.
[81] K.X. Tu, F.Y. Li, Z.F. Chen, J. Mater. Res. 31 (2016) 878–885.
[82] W.F. Li, Y.G. Mu, Nanoscale 4 (2012) 1154–1159.
[83] J.B. Goodenough, Y. Kim, Chem. Mater. 22 (2010) 587–603.
[84] N. Nitta, G. Yushin, Part. Part. Syst. Char. 31 (2014) 317–336.
[85] Q.X. Zhang, C.M. Tang, L. Fu, Appl. Surf. Sci. 497 (2019) 143723.
[86] Y.D. Yu, Z.L. Guo, Q. Peng, J. Zhou, Z.M. Sun, J. Mater. Chem. A 7 (2019) 12145–12153.
[87] X. Zhang, Z.H. Zhang, S. Yao, et al., Npj Comput. Mater. 4 (2018) 13.
[88] D. Datta, J.W. Li, V.B. Shenoy, ACS Appl. Mater. Inter. 6 (2014) 1788–1795.
[89] F. Li, Y.Y. Qu, M.W. Zhao, J. Mater. Chem. A 4 (2016) 8905–8912.